Imperial College London

Imperial College London

Department of Physics

Quantum Field Theory on 3D Causal Sets

Author:

Shivraj Jalan

Supervisor:

Yasaman Yazdi

Submitted in partial fulfillment of the requirements for the MSc degree in Quantum Fields and Fundamental Forces at the Imperial College London

September 2021

Abstract

In this thesis we introduce the causal set approach to quantum gravity and review the formalism for doing scalar quantum field theory on a causal set. We then look at the Sorkin-Johnston (SJ) ground state of a two dimensional causal diamond and review work done on exploring this vacuum state on two subregions, the center and wedge. In the two dimensional case, it was found that although the SJ vacuum resembled the Minkowski vacuum in the center of the causal diamond, it did not resemble the expected Rindler vacuum on the wedge. Instead the SJ vacuum in this region resembled the ground state of a scalar field with reflecting boundary conditions at the corner, resembling mirror behavior. We explore this result further in the case of a three dimensional causal diamond and mention preliminary results indicating that this may also be the case in three dimensions.

Contents

Chapter 1

Causal Sets

1.1 Introduction

The great challenge today in theoretical physics involves finding a unified description of two distinct theories, quantum mechanics and general relativity, merging them into a single theory of quantum gravity. On the one hand, quantum theory makes astounding predictions at the smallest scales while on the other, general relativity provides a framework for understanding space-time at the largest. At the heart of this search is the question regarding the nature of space-time, whether it is fundamentally discrete or continuous. As pointed out by 't Hooft [1], many of the divergences that arise in quantum field theory can be avoided by starting with a framework where space-time is viewed as a collection of discrete points satisfying a causal order. Traditionally continuum space-time is viewed as a manifold endowed

with a differentiable structure given by the metric, however in the discrete case the metric is replaced by causal relationships between discrete space-time points. Building on this movement towards discreteness, a possible approach to a unified theory of quantum gravity is that of causal sets, first proposed by Bombelli, Lee, Meyer and Sorkin (BLMS) [5], and inspired in part by earlier work by authors including Hawking, King and McCarthy [9], as well as Malament [16], 't Hooft [1] and Myrheim [17]. The starting point here is the discrete set of space-time points with a causal structure imposed on them. The causal order is determined by asking whether each point sits in the future or past light cone with respect to other points in the set. As mentioned in [1], this is enough to determine the continuum metric tensor up to a conformal factor that is related to the volume of space-time [5]. Similar approaches have also been explored in the past dating back to Riemann [7] and revisited by authors such as Zeeman [27], Hemion [10] and Finkelstein [8]. Other important results regarding the causal structure were also demonstrated by Hawking [9], Malament [16] and Levichev [15], culminating in the Hawking-King-McCarthy-Malament (HKMM) theorem. This states that if a chronological bijection exists between two d-dimensional space-times that are both future and past distinguishing, then these space-times must be conformally isometric for $d > 2$ [25]. What this means for causal sets is that if the volume is determined by the number of causal set points, while each point satisfies a causal order with respect to the others, then this is enough to fully describe a Lorentzian geometry. This is summarised in the slogan "Order +

Number = Geometry". Since the paper by BLMS, research into causal sets has branched out in several directions, where in particular, scalar quantum field theory was developed in this framework building on work done by Steven Johnston [14]. As the traditional quantisation approach does not work for discrete causal sets, work was done to formally define a vacuum state for a free scalar quantum field theory on a causal set, leading to a suggestion for a distinguished ground state by Sorkin, Aslanbeigi and Afshordi [2], called the Sorkin-Johnston (SJ) vacuum. This proposal was then tested in the case of a two dimensional causal diamond to determine whether the SJ vacuum is indeed consistent with the vacuum state predicted by the traditional quantisation approach [3]. This will be of particular relevance to this thesis as, following an initial introduction to causal set theory, we review work done in [3]. We ultimately want to explore the vacuum states of a free scalar quantum field theory on a causal diamond in three space-time dimensions. In this thesis, the metric convention we will be using is $(-+++)$, following [3].

1.2 Basic Definitions

In this section we formally introduce key definitions that will be referred back to frequently in later chapters. The definitions introduced in this section follow the formalism established in [5][14][25].

1.2.1 Partial Orders, Causal Sets and Embeddings

We start off by defining relations and partially ordered sets. A *relation* R on a set S is the subset of $S \times S$, where '$\times$' denotes the cartesian product of two sets of ordered pairs of elements $(s, t) \in S$, where we write sRt to denote s is R-related to t. A *partially ordered set (poset)* is a set S together with a relation R that satisfies the following properties [14],

(i) $\forall s \in S,\ sRs$ (Reflexive)

(ii) $\forall s, t \in S,\ sRtRs \implies s = t$ (Antisymmetric)

(iii) $\forall s, t, u \in S,\ sRtRu \implies sRu$ (Transitive)

A *causal set* is then a poset with the additional requirement that it is locally finite [5]. Hence it is defined as a pair $(C, \preceq)$, where C is a set and the relation R is replaced with $\preceq$, the partial order, such that the elements $u, v, w \in C$ satisfy the following properties [5],

(i) $\forall u \in C, u \preceq u$ (Reflexive)

(ii) $\forall u, v \in C$, if $u \preceq v$ and $v \preceq u$, then $u = v$ (Antisymmetric)

(iii) $\forall u, v, w \in C$ if $u \preceq v$ and $v \preceq w$, then $u \preceq w$ (Transitive)

(iv) $\forall u, v \in C$, $|[u, v]| < \infty$ (Locally finite)

If $\forall u, v \in C,\ u \preceq v$ and $u \neq v$, we write $u \prec v$ so u strictly precedes v. Additionally, if u, v have no causal relationship as they may, for example, lie

outside each other's light cones, we write $u||v$. In other words, a causal set is a set of space-time points with a causal relation between them, depending on whether or not they lie inside each other's light cones. In the last condition we define the *Causal Interval* or *Alexandrov Set* as the set,

$$[u, v] := \{w \in C : u \preceq w \preceq v\} \text{ for } u \preceq v \tag{1.1}$$

Hence it is the last condition that highlights space-time discreteness as it adds the condition that the cardinality of the causal interval between any two causal set points must be finite [14]. To understand how large causal sets approximate the continuum Lorentzian manifold structure, we need to define the notion of an embedding. If $(C, \preceq)$ is a causal set, an *embedding* of a causal set into a Lorentzian manifold (M, g) is defined as a map $f : C \to M$ such that $x \preceq y \iff f(x) \preceq f(y)$. Additionally, a *faithful embedding* is an embedding where the image of the causal set points under f are uniformly distributed in M according to the volume measure on M [14][25]. There are causal sets, however, that don't exhibit manifold like structure on the large scale, and the precise dynamics that lead to suppressing these is not fully understood [13]. An important conjecture related to embeddings, referred to as the *Hauptvermutang* of causal set theory, states that if a causal set can be faithfully embedded into two distinct space-times (M, g) and (M', g'), then these two space-times must be approximately isometric [25]. In order to generate causal sets that faithfully embed in a given Lorentzian manifold,

we use a process called sprinkling. By sprinkling, we mean generating points on the Lorentzian manifold so that they are Poisson distributed, where the probability of finding n points in a space-time volume V is given by,

$$P(\text{n points in volume V}) = \frac{(\rho V)^n}{n!} e^{-\rho V}$$

where ρ is the sprinkling density [14]. The Poisson distribution prevents causal set points from picking out a particular direction in space-time, whilst also allowing the statistical distribution to be invariant under Lorentz boosts [11]. We see an example of such a spinkling in Figure 1.1 below.

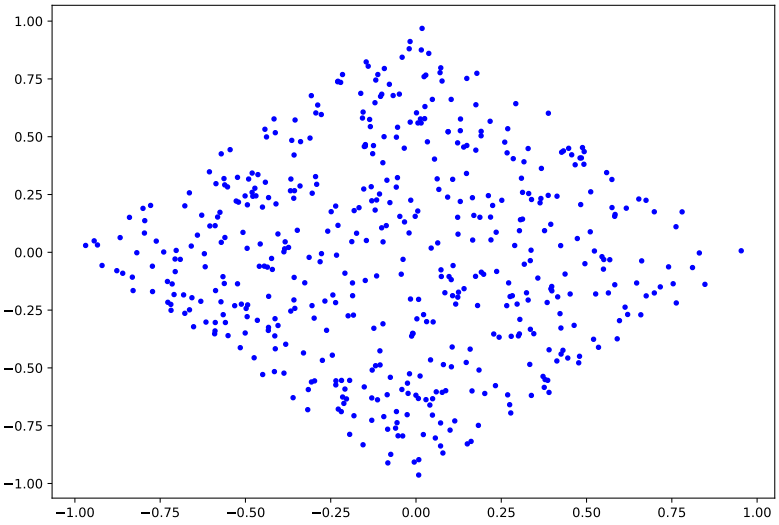

Figure 1.1: A sprinkling into a 2D causal diamond with $N = 500$ points.

1.2.2 Chains, Links and Paths

We can label the elements v_i of a causal set C by assigning them indices $i \in 1, ..., |C|$. A labelling is a natural labelling if $v_i \preceq v_j \implies i \leq j$. A set is *totally ordered* if there is a partial order between all pairs of elements in the set. An interesting point to note is that the labelling one chooses is the analogue of a choice of coordinate system in the continuum [25]. We now define the important notions of chains, multichains and antichains following [14]. A chain is a sub-poset of the causal set $(C, \preceq)$ that is totally ordered. A chain of length n is given by a sequence of elements $u_0 \prec u_1 \prec ... \prec u_n$ where $u_i \in C$ for all $i \in [1, .., n]$, while a *multichain* is a chain with repeated elements. An important point that will be useful when we start looking at propagators is that the length of the longest chain between two points in a causal set is proportional to the proper time between them [25]. An *antichain* is a set of elements in the causal set which are mutually causally unrelated. A *link* is a relation $u \prec v$ such that there exists no element w where $u \prec w \prec v$. If this is the case we define u and v as *nearest neighbors*, denoted by $u \prec *v$. A *path* is a subset $P \subset C$ such that given $u, v \in P$, there exists no element $w \in C - P$ such that $u \prec w \prec v$. A path of length n is a sequence of distinct elements $u_0 \prec *u_1 \prec *... \prec *u_n$. We can encode the causal relationships between points in the causal set via the *causal matrix*. If we have a causal

set $(C, \preceq)$ with p elements, the causal matrix C is defined as,

$$C_{xy} := \begin{cases} 1 \text{ if } v_x \prec v_y \\ 0 \text{ otherwise.} \end{cases} \tag{1.2}$$

where $x, y \in [1, ..., p]$. We also define the *link matrix* on a causal set by,

$$L_{xy} := \begin{cases} 1 \text{ if } v_x \prec *v_y \\ 0 \text{ otherwise.} \end{cases} \tag{1.3}$$

We can always use a natural labelling to index points in the causal set so that both the causal and link matrices become strictly upper triangular. The way we do this is by ordering points by their time coordinate. We can visualise a causal set through the use of a *Hasse diagram* as depicted in Figure 1.2 [14]. Figure 1.2 (a) depicts the causal links between points in a causal set made up of six elements, $\{v_1, ..., v_6\}$, while (b) highlights the full causal structure. We can use these diagrams to read off the entries of the causal and link matrices respectively. A path can be visualised as a route drawn between points in (a), while in (b) this would be called a chain. The corresponding link and causal matrices, denoted by L and C respectively, would in this case be given

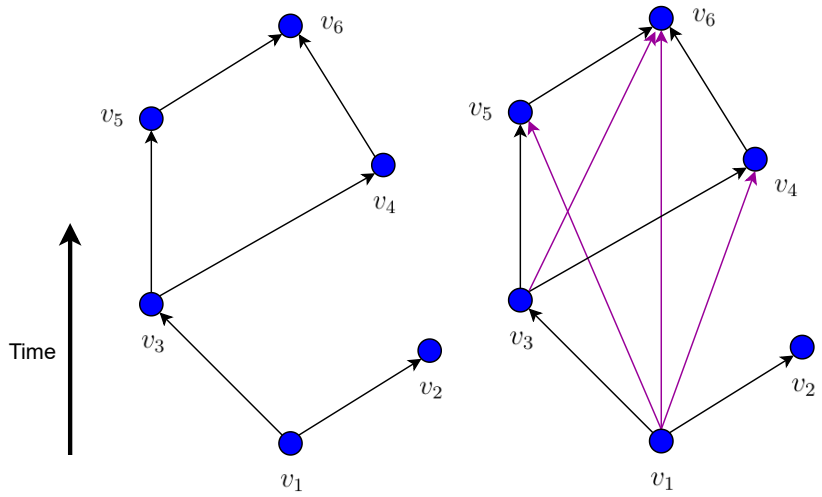

(a) Link diagram (b) Causal diagram

Figure 1.2: Hasse diagrams of Link and Causal matrices.

by,

$$L = \begin{pmatrix} 0 & 1 & 1 & 0 & 0 & 0 \\ 0 & 0 & 0 & 0 & 0 & 0 \\ 0 & 0 & 0 & 1 & 1 & 0 \\ 0 & 0 & 0 & 0 & 0 & 1 \\ 0 & 0 & 0 & 0 & 0 & 1 \\ 0 & 0 & 0 & 0 & 0 & 0 \end{pmatrix} \qquad C = \begin{pmatrix} 0 & 1 & 1 & 1 & 1 & 1 \\ 0 & 0 & 0 & 0 & 0 & 0 \\ 0 & 0 & 0 & 1 & 1 & 1 \\ 0 & 0 & 0 & 0 & 0 & 1 \\ 0 & 0 & 0 & 0 & 0 & 1 \\ 0 & 0 & 0 & 0 & 0 & 0 \end{pmatrix} \tag{1.4}$$

We can see that, as the points in the figure are labelled by their time index, we do indeed get upper triangular matrices for L and C. The causal and link matrices are the crucial starting point for any kind of analysis on causal sets, and form the basis for defining the Greens function, or propagator, in scalar quantum field theory on causal sets. As such we will state some useful results

regarding the entries of powers of the causal and link matrices [14][24].

$$(C^n)_{xy} = \text{Number of chains of length } n \text{ from } v_x \text{ to } v_y. \tag{1.5}$$

$$(L^n)_{xy} = \text{Number of paths of length } n \text{ from } v_x \text{ to } v_y. \tag{1.6}$$

Using this we see that the entries of $(C)_{xy}$ and of $(C^2)_{xy}$ represent the number of chains of length one and two from point v_x to v_y respectively. Hence we know that if we have a non-zero entry in the (x, y) position of the C^2 matrix, v_x and v_y could not have been nearest neighbors. As a result we conclude that $L_{xy} = C_{xy} - \mathbb{1}_{\{(C^2)_{xy}>0\}}$, where the indicator function is defined as,

$$\mathbb{1}_A = \begin{cases} 1 \text{ if } A \\ 0 \text{ if } A^c. \end{cases} \tag{1.7}$$

for the event $A = \{(C^2)_{xy} > 0\}$. Finally, we also note that we can calculate the volume of the causal interval between two points in the causal set $v_x, v_y \in (C, \preceq)$ directly from the causal matrix using the equation [14],

$$V_{xy} = \frac{1}{\rho}(C + I)^2_{xy} \tag{1.8}$$

After establishing these basic definitions, we can now look at how one can start doing quantum field theory on causal sets.

1.3 QFT on Causal Sets

In this chapter we aim to establish the formalism for doing quantum field theory on a causal set. We start by briefly reviewing how free scalar quantum field theory works in the traditional, continuum approach for a flat Minkowski space-time. Then, following Johnston's formalism, we see what the analogue would be in the case of causal sets.

1.3.1 Continuum Free Scalar QFT

For a free classical scalar field theory in a flat d-dimensional Minkowski space-time with coordinates $x = (t, \boldsymbol{x})$, the equations of motion are given by the Klein-Gordon equations,

$$(\Box - m^2)\phi(x) = 0 \tag{1.9}$$

where $\Box$ stands for the d'Alembert operator $\partial^\mu \partial_\mu = (-\partial_t^2, \boldsymbol{\nabla}^2)$. We can obtain the solution for $\phi(x)$ in terms of it's Fourier coefficient expansion,

$$\phi(x) = \int d^d\widetilde{\boldsymbol{k}} \left(a(\boldsymbol{k}) e^{-ikx} + a^\dagger(\boldsymbol{k}) e^{ikx} \right) \tag{1.10}$$

where the measure $d^d\widetilde{\boldsymbol{k}} = \frac{d^d\boldsymbol{k}}{(2\pi)^d 2E(\boldsymbol{k})}$. To then go from a classical field theory to quantum, we promote $\phi(x)$ to an operator valued field $\hat{\phi}(x)$ resulting in the Fourier coefficients also being promoted to the operators $\hat{a}(\boldsymbol{k})$ and $\hat{a}^\dagger(\boldsymbol{k})$

respectively. Together with the canonical commutation relation,

$$\left[\hat{\phi}(t,\boldsymbol{x}),\frac{\partial\hat{\phi}(t,\boldsymbol{y})}{\partial t}\right]=i\delta^{d}(\boldsymbol{x}-\boldsymbol{y}) \tag{1.11}$$

this defines a vacuum state $|0\rangle$ as the state annihilated by the positive frequency Fourier modes of $\hat{\phi}(x)$ [23] so that,

$$\hat{a}(\boldsymbol{k})\,|0\rangle=0 \tag{1.12}$$

From this we can construct the usual Fock space by acting on the vacuum state with creation operators to obtain general states of the form [26],

$$|\boldsymbol{k}_1...\boldsymbol{k}_n\rangle=\hat{a}^{\dagger}(\boldsymbol{k}_1)...\hat{a}^{\dagger}(\boldsymbol{k}_n)\,|0\rangle \tag{1.13}$$

1.3.2 The Continuum Propagator

Next we define the retarded Greens function of the Klein-Gordon operator as the function $G_R(x)$ that satisfies the equation,

$$(\Box-m^2)G_R(x)=\delta^{(d)}(x) \tag{1.14}$$

Additionally, G_R has the boundary conditions that it is only non-zero in the future light cone [14]. From G_R we can also define the advanced Greens function as $G_A(x)=G_R(-x)$, which thus must have the boundary condition

that it is only non-zero in the past light cone. Writing $\delta^d(x)$ as,

$$\delta^{(d)}(x) = \frac{1}{(2\pi)^d} \int d^d k \; e^{ikx} \tag{1.15}$$

where $k = (k_0, \boldsymbol{k})$, we see that inverting Equation 1.14 we have,

$$\begin{aligned} G_R(x) = \frac{1}{(\Box - m^2)} \delta^{(d)}(x) &= \frac{1}{(2\pi)^d} \int d^d k \; \frac{1}{(\Box - m^2)} e^{ikx} \\ &= \frac{1}{(2\pi)^d} \int d^d k \; \frac{e^{ikx}}{(-k^2 - m^2)} \\ &= \frac{1}{(2\pi)^d} \int d^d k \; \frac{e^{ikx}}{(k_0^2 - \boldsymbol{k}^2 - m^2)} \end{aligned} \tag{1.16}$$

We can then write the d-dimensional Minkowski space-time Klein-Gordon propagator more formally as [14],

$$(G_R)^{(d)}_m(x) = \lim_{\epsilon \to 0^+} -\frac{1}{(2\pi)^d} \int d^d k \frac{e^{-ikx}}{(k_0 + i\epsilon)^2 - \boldsymbol{k}^2 - m^2} \tag{1.17}$$

where now we include the $i\epsilon$ term, as the k_0 integral is in fact a contour integral in the complex plane around the poles at $k_0 = \pm\sqrt{\boldsymbol{k}^2 + m^2}$, and hence to evaluate this integral we need to shift the integrand slightly away from the poles. The index m and d make explicit the mass and dimension dependence of $G_R(x)$. In order to make the comparison between the causal set and continuum propagators later, we will need the explicit forms for these

Greens functions in various dimensions. These are listed in [14] as,

$$(G_R)_m^{(1)}(x) = \theta(x^0)\frac{\sin(mx^0)}{m} \tag{1.18}$$

$$(G_R)_m^{(2)}(x) = \theta(x^0)\theta(\tau^2)\frac{1}{2}J_0(m\tau) \tag{1.19}$$

$$(G_R)_m^{(3)}(x) = \theta(x^0)\theta(\tau^2)\frac{1}{2\pi}\frac{\cos(m\tau)}{\tau} \tag{1.20}$$

$$(G_R)_m^{(4)}(x) = \theta(x^0)\theta(\tau^2)\left(\frac{1}{2\pi}\delta(\tau^2) - \frac{m}{4\pi}\frac{J_1(m\tau)}{\tau}\right) \tag{1.21}$$

where $\tau = \sqrt{-(x^0)^2 + \boldsymbol{x}^2}$ is the proper time, $J_\alpha(x)$ is the Bessel function of the first kind, and $\theta(x)$ is the heavy-side function defined as,

$$\theta(x) = \begin{cases} 1 & \text{for } x \geq 0 \\ 0 & \text{for } x < 0 \end{cases}$$

As we will focused on massless free scalar field theory, we will primarily be using the massless versions of these expressions. The Greens function can also be interpreted as the propagator between two space-time points x and x' satisfying the equation,

$$(\Box - m^2)G_R(x, x') = \delta^{(d)}(x - x') \tag{1.22}$$

By using a similar process, we can invert Equation 1.22 and integrate over the k_0 variable to find the explicit expression for $G_R(x, x')$ as

$$G_R(x, x') = i \int d^d\widetilde{\boldsymbol{k}} \left(e^{-ik(x-x')} - e^{ik(x-x')} \right) \tag{1.23}$$

Using the Greens function in this form, we can then define the *Pauli-Jordan function*, $\Delta(x, x')$, as the difference between the retarded and advanced Greens functions [12],

$$\Delta(x, x') = G_R(x, x') - G_A(x, x') \tag{1.24}$$

This will play a central role in the alternative definition of the vacuum state introduced in chapter two. Equation 1.11 imposes the condition,

$$\left[\hat{a}(\boldsymbol{k_1}), \hat{a}^\dagger(\boldsymbol{k_2})\right] = (2\pi)^d 2E(\boldsymbol{k_1})\delta^d(\boldsymbol{k_1} - \boldsymbol{k_2}) \tag{1.25}$$

on the Fourier coefficients, while all other commutators give us zero. Using this we can calculate the commutator $\left[\hat{\phi}(x), \hat{\phi}(x')\right]$ given by,

$$\left[\int d^d\widetilde{\boldsymbol{k_1}} \left(\hat{a}(\boldsymbol{k_1}) e^{-ik_1 x} + \hat{a}^\dagger(\boldsymbol{k_1}) e^{ik_1 x} \right), \int d^d\widetilde{\boldsymbol{k_2}} \left(\hat{a}(\boldsymbol{k_2}) e^{-ik_2 x'} + \hat{a}^\dagger(\boldsymbol{k_2}) e^{ik_2 x'} \right) \right] \tag{1.26}$$

which results in the final expression,

$$\left[\hat{\phi}(x), \hat{\phi}(x')\right] = \int d^d\widetilde{\boldsymbol{k}} \left(e^{-ik(x-x')} - e^{ik(x-x')} \right) = i\Delta(x, x') \tag{1.27}$$

Finally, the *Wightman* or *two-point function*, $W(x, x')$, is defined in terms of the vacuum expectation value,

$$\langle 0| \hat{\phi}(x)\hat{\phi}(x') |0\rangle = W(x, x') \tag{1.28}$$

From Equation 1.27, it is easy to see that the relationship between the Wightman function and the Pauli-Jordon function is given by [21],

$$i\Delta(x, x') = \langle 0| [\hat{\phi}(x), \hat{\phi}(x')] |0\rangle = W(x, x') - W(x', x) \tag{1.29}$$

For "Gaussian" theories, the Wightman function can be used to determine all higher order correlation functions, and will play a central role in determining the ground state of a scalar quantum field theory on a causal set [23].

1.3.3 QFT on causal sets

To transition from continuum quantum field theory to the discrete, causal set version, we begin by reviewing the model introduced in [14]. We start by sprinkling a causal set into a Lorentzian manifold and imagine a particle initially at rest at some space-time point within this causal set. It can move through the causal set by jumping from one causally related point to another, resting for some time after each jump. The process of jumping is called a 'hop' and has a probability amplitude a, while when it's resting it's a 'stop', with amplitude b, hence the name 'Hop and Stop Model' [14]. The particle

travels along a trajectory which is either on chains or on links within the causal set, and we imagine it hops n times and stops $n-1$ times. The total probability amplitude for this trajectory is then $a^n b^{n-1}$. In this model the hopping and stopping amplitudes are constant and independent of the path taken. This gives a Markov chain process for the particle hopping between points in the causal set, where, depending on whether we sum over chains or paths, the transition matrices of these processes are given by either $\Phi = aC$ or $\Phi = aL$, where C and L are the causal and link matrices respectively. If the causal set has p elements then C and L must both be $p \times p$ matrices. Additionally, as with all probability transition matrices, the entries of $(\Phi^n)_{xy}$, the n^{th} power of the transition matrix, gives the probability that a particle starting at v_x ends up at v_y after n hops. If we include the $n-1$ stops, this is given by the matrix elements $(b^{n-1}\Phi^n)_{xy}$. Hence to get an expression for the total probability K_{xy} of a particle going from v_x to v_y in the causal set, we sum over all possible hop lengths n,

$$K_{xy} = (\Phi + b\Phi^2 + b^2\Phi^3 + ...)_{xy} = \left(\sum_{n=1}^{\infty} b^{n-1}\Phi^n\right)_{xy} \tag{1.30}$$

As Φ is strictly upper triangular[1] it must be nil-potent, guaranteeing the terms in the summation eventually terminate. Thus we can use the sum of

[1]Recall this is always possible when the causal set elements are defined through natural labelling.

a geometric series formula to rewrite K as,

$$K = \Phi(I - b\Phi)^{-1} \tag{1.31}$$

where explicitly in the case of propagation over chains we have,

$$K = aC(I - abC)^{-1} \tag{1.32}$$

The values for a and b are set so that K matches the known results for the retarded Klein-Gordon propagator in ordinary continuum scalar quantum field theory. Johnston gives these as $a = A\rho^{1-\frac{2}{d}}$ and $b = \frac{-m^2}{\rho}$, using an argument employing dimensional analysis [14], where ρ is once again the causal set sprinkling density, A is a constant and d is the space-time dimension. To make the comparison with the continuum, we see that the causal set version of the propagator in Equation 1.31 is identified as the analogue of the retarded Greens function G_R in the continuum, and so is actually the retarded causal set propagator $K = K_R$. We also get the analogous advanced propagator K_A, from K_R, using that $K_A = (K_R)^T$, which is the matrix equivalent of $G_A(x, x') = G_R(x', x)$. The causal set version of the continuum Pauli-Jordan function $\Delta(x)$ is then similarly defined as [12],

$$\Delta = K_R - K_A \tag{1.33}$$

where this is now a matrix equation due to the discreteness of the causal set. We will be mainly interested in a slightly modified version of the Pauli-Jordon function, $i\Delta$, which as we saw earlier in Equation 1.27, is equated to the commutator between two operator valued free scalar fields. From Equation 1.27 we also see that $i\Delta(x, y)$ is split into a positive and negative frequency part, where the positive frequency part is defined to be the Wightman function. This will also turn out to be the case in the discrete case, where the 'positive frequency' part is defined in terms of the spectral decomposition of $i\Delta$. First we note some properties of $i\Delta$. It is antisymmetric,

$$(i\Delta)^T = i(K_R^T - K_A^T) = i(K_A - K_R) = -i\Delta \tag{1.34}$$

as well as Hermitian,

$$(i\Delta)^\dagger = -i(\Delta)^\dagger = -i(\Delta)^T = i\Delta \tag{1.35}$$

where we have used that $\Delta^\dagger = \Delta^T$ as Δ is a real matrix. Using these two properties we infer the eigenvalues of $i\Delta$ must be real due to Hermiticity and come in positive and negative pairs due to antisymmetry. We can thus write the eigenvalue equation for $i\Delta$ as [14],

$$i\Delta u_i^\pm = \pm\lambda u_i^\pm \tag{1.36}$$

where $u_i^{\pm}$ are the normalised eigenvectors corresponding to the pair of eigenvalues $\pm\lambda > 0$, while the indices $i \in [1, .., l]$ for $r = 2l$, where r is the rank of $i\Delta$. The eigenvectors $u_i^{\pm}$ also satisfy the conditions [12],

$$u_i^+ = (u_i^-)^* \quad u_i^+(u_j^+)^\dagger = u_i^-(u_j^-)^\dagger = \delta_{ij} \quad u_i^+(u_j^-)^\dagger = 0 \tag{1.37}$$

due to the Hermiticity and antisymmetry of $i\Delta$. We can then expand $i\Delta$ using spectral decomposition to get,

$$i\Delta = \sum_{i=1}^{l} \lambda_i (u_i^+)(u_i^+)^\dagger - \sum_{i=1}^{l} \lambda_i (u_i^-)(u_i^-)^\dagger \tag{1.38}$$

This can also alternatively be written as $i\Delta = UDU^\dagger$, where U is the matrix of eigenvectors and D a diagonal matrix with the corresponding eigenvalues on the diagonal. The causal set Wightman function w is then defined as the positive part of the spectral decomposition of $i\Delta$,

$$w = \sum_{i=1}^{l} \lambda_i (u_i^+)(u_i^+)^\dagger \tag{1.39}$$

and hence we can write $i\Delta = w - w^T$ [14]. We can also write w in matrix form as $w = UD^+U^\dagger$, where D^+ is now the original diagonal eigenvalue matrix D with all eigenvalues less than zero set to zero so that D^+ only contains the positive eigenvalues of w. The causal set version of the scalar field operator can also be given by an algebra of field operators $\hat{\phi}_x$ for each one of the p causal set elements v_x acting on a Hilbert space H. These field operators

must satisfy the conditions [14],

1. $\hat{\phi}_x = \hat{\phi}_x^\dagger$

2. $[\hat{\phi}_x, \hat{\phi}_y] = i\Delta_{xy}$

3. $i\Delta w = 0 \implies \sum_{j=1}^{p} w_j \hat{\phi}_j = 0$

For a p-component complex vector w. We can write the causal set field operator $\hat{\phi}_x$ as [12],

$$\hat{\phi}_x = \sum_{i=1}^{l} (u_i^+)_x \hat{a}_i + (u_i^-)_x \hat{a}_i^\dagger \tag{1.40}$$

where $\hat{a}_i$ and $\hat{a}_i^\dagger$ are the creation and annihilation operators satisfying similar commutation relations as those in the continuum case,

$$[\hat{a}_i, \hat{a}_j] = 0 \quad [\hat{a}_i^\dagger, \hat{a}_j^\dagger] = 0 \quad [\hat{a}_i, \hat{a}_j^\dagger] = \lambda_j \delta_{ij} \tag{1.41}$$

The creation and annihilation operators written in terms of $\hat{\phi}_x$ are [12],

$$\hat{a}_i = \sum_{x=i}^{p} (u_i^-)_x \hat{\phi}_x \quad \hat{a}_i^\dagger = \sum_{x=i}^{p} (u_i^+)_x \hat{\phi}_x \tag{1.42}$$

As in the continuum case, the vacuum state $|0\rangle \in H$ is defined as the state annihilated by the $\hat{a}_i$ operators so that $\hat{a}_i |0\rangle = 0$ and is normalised so that $\langle 0|0\rangle = 1$. H is then the Fock space spanned by basis vectors of the form $(\hat{a_1}^\dagger)^{n_1}(\hat{a_2}^\dagger)^{n_2}...(\hat{a_l}^\dagger)^{n_l} |0\rangle$ for positive integers n_i. We can check that this formulation gives the correct causal set Wightman function w_{xy} by calculating

the two point correlator in terms of the causal set fields $\hat{\phi}_x$ and $\hat{\phi}_y$ so that [12],

$$\begin{aligned}
\langle 0|\, \hat{\phi}_x \hat{\phi}_y \,|0\rangle &= \sum_{i=1}^{l}\sum_{j=1}^{l} (u_i^+)_x (u_j^-)_y \,\langle 0|\, \hat{a}_i \hat{a}_j^\dagger \,|0\rangle \\
&= \sum_{i=1}^{l}\sum_{j=1}^{l} (u_i^+)_x (u_j^-)_y \,\langle 0|\, [\hat{a}_i, \hat{a}_j^\dagger] \,|0\rangle \\
&= \sum_{i=1}^{l}\sum_{j=1}^{l} (u_i^+)_x (u_j^+)_y^* \lambda_j \delta_{ij} \\
&= \left(\sum_{i=1}^{l} \lambda_i (u_i^+)(u_i^+)^\dagger \right)_{xy} = w_{xy}
\end{aligned} \tag{1.43}$$

where in the third line we used the first condition of (1.37). Hence we see that this formalism is consistent with what we would expect from Equation 1.39. As we will see in the following chapter, the Pauli-Jordan function and the Wightman function play a key role in establishing an alternative definition of the ground state of a free scalar quantum field theory, both in the continuum and causal set frameworks.

Chapter 2

The Ground State

In this chapter we will look more closely at how the ground, or vacuum state is defined in a free scalar quantum field theory and look at the alternative proposal made in [2] following work done in [23] [14]. We will begin by reviewing this proposal in the continuum case and see how the definitions naturally carry over to causal sets. We then review work done in [3] with the aim of understanding the vacuum state on two subregions of a two dimensional causal diamond in Minkowski space.

2.1 The Ground State in Scalar QFT

As we saw in the previous chapter, the vacuum state of a quantum field theory can be defined as the state annihilated by the positive frequency Fourier modes. An alternative way to characterise the vacuum state however, is to

define it through it's correlation functions, in particular using the Wightman function, as all higher order correlations are determined by this in a free Gaussian theory. As we also saw, the Wightman function can be obtained from the positive frequency part of $i\Delta$, which in turn is defined through the retarded Greens propagator G_R. This chain of ideas was used by Sorkin in [23] and developed further in [2] to specify a unique vacuum state for a quantum field theory in more general curved space-times, called the Sorkin-Johnston (SJ) vacuum. Defining the vacuum state in this way is beneficial for several reasons. First, it doesn't require the notion of positive frequencies or symmetries and hence can be used to define a vacuum state in arbitrary curved space-times. Additionally, it is manifestly covariant as it only works with space-time quantities. Finally, defining the vacuum state in this way will be particularly useful to causal sets as the notion of positive frequencies isn't well defined and hence traditional quantisation wouldn't work. Following [2], we start off by generalising the equations from the previous section to curved space-times. Thus ϕ is now viewed as a real valued scalar field on a hyperbolic space-time $(M, g_{\mu\nu})$ and the operator ∂_μ transforms as $\partial_\mu \to \nabla_\mu$, the covariant derivative operator on M. The Klein-Gordon equation then becomes,

$$\left(\nabla^\mu \nabla_\mu + m^2\right) \phi(x) = 0 \tag{2.1}$$

where the mass m is non-negative. Additionally the retarded and advanced Greens functions $G_{R,A}$ now satisfy the equations,

$$\left(\nabla^{\mu}\nabla_{\mu} + m^2\right) G_{R,A}(x, x') = -\frac{\delta^{(d)}(x - x')}{\sqrt{-g}} \tag{2.2}$$

where g is the determinant of the metric tensor $g_{\mu\nu}$. The Pauli-Jordan function $\Delta(x, x')$ has the same form as in Equation 1.24, and we now use it to define the integral operator [2],

$$\left(\Delta f\right)(x) \equiv \int_M \Delta(x, x') f(x')\ dV_{x'} \tag{2.3}$$

where $dV_{x'} = \sqrt{-g(x')} d^d x'$ is the volume measure on M. We also note that as $\Delta(x, x')$ is the difference of two Greens functions it trivially satisfies the Klein-Gordon equation [2],

$$\left(\Box + m^2\right) \Delta = 0 \tag{2.4}$$

Once again we go to the quantum theory by promoting ϕ to an operator $\hat{\phi}$, and the canonical commutation relations now take the form,

$$\left[\hat{\phi}(x), \hat{\phi}(x')\right] = i \int_M f(x) \Delta(x, x') f(x')\ dV_x dV_{x'} \tag{2.5}$$

which in short hand can be written as [23],

$$\left[\hat{\phi}(x), \hat{\phi}(x')\right] = i\Delta \tag{2.6}$$

$i\Delta(x, x')$ is again Hermitian and antisymmetric as we saw before, and so it's eigenvalues must again be real and come in positive and negative pairs.

2.2 The SJ Vacuum

The Sorkin Johnston (SJ) vacuum is defined in terms of the Pauli-Jordan function $i\Delta$, as the state $|SJ\rangle$, such that $\langle SJ| \hat{\phi}(x)\hat{\phi}(x') |SJ\rangle = Pos(i\Delta(x, x'))$, where $Pos(i\Delta(x, x'))$ is the positive spectral projection of $i\Delta$ through the spectral theorem. We view $i\Delta$ as an operator acting on the Hilbert space of square integrable functions $L^2(M, dV)$ [2]. The "ground state condition" is then interpreted as defining the two-point function $W_{SJ}(x, x')$ to be the positive part of the Pauli-Jordon function so that $W_{SJ}(x, x') = Pos(i\Delta(x, x'))$. For a free scalar field in a d-dimensional globally hyperbolic spacetime $(M, g_{\mu\nu})$, the Wightman function W_{SJ} of the SJ state is defined by the three conditions [3][23],

1. $i\Delta = \left[\hat{\phi}(x), \hat{\phi}(x')\right] = W_{SJ}(x, x') - W^*_{SJ}(x', x)$ (Commutator)

2. $\int_M \int_M f^*(x) W_{SJ}(x, x') f(x')\ dV_x dV_{x'} \geq 0$ (Positivity)

3. $\int_M W_{SJ}(x, x') W^*_{SJ}(x', x'')\ dV_{x'} = 0$ (Orthogonal Support)

where once again $dV_x = d^dx\sqrt{-g(x)}$. It can also be shown that W_{SJ} is unique and hence these conditions specify the state fully [3]. We can slightly modify the integral operator in (2.3) and define it to be the Pauli-Jordan operator $i\Delta$ on $L^2(M, dV)$,

$$(i\Delta f)(x) = \int_M dV_{x'} i\Delta(x, x') f(x') \tag{2.7}$$

where the inner product on $L^2(M, dV)$ is given by,

$$\langle f, g\rangle = \int_M dV f(x)^* g(x) \tag{2.8}$$

Analogous to the causal set case in the previous chapter, we can use the Hermiticity and antisymmetry of $i\Delta$ to write the eigenvalue equation [3],

$$(i\Delta T_q^{\pm})(x) = \pm\lambda_q T_q^{\pm}(x) \tag{2.9}$$

where q indexes the set of eigenfunctions, while $T_q^-(x) = \left[T_q^+(x)\right]^*$ and $\lambda_q > 0$ for all q. The spectral decomposition of the Pauli-Jordan operator is similarly,

$$i\Delta(x, x') = \sum_q \lambda_q T_q^+(x) T_q^+(x')^* - \sum_q \lambda_q T_q^-(x) T_q^-(x')^* \tag{2.10}$$

where we also assume the eigenfunctions $T_q^{\pm}$ are L^2-normalised so that $||T_q^{\pm}||^2 = \left\langle T_q^{\pm}, T_q^{\pm}\right\rangle = 1$. Now $W_{SJ}(x, x') = Pos(i\Delta(x, x')$ is then just the first term on

the right hand side of this expression,

$$W_{SJ}(x,x') = \sum_q \lambda_q T_q^+(x) T_q^+(x')^* = \sum_q \tau_q(x)\tau_q(x') \tag{2.11}$$

where $\tau_q(x) = T_q^+(x)\sqrt{\lambda_q}$. The ground state defined in this way provides a consistent definition for the vacuum state in both the causal set and continuum framework. The discrete nature of causal sets provides the added benefit that the operators mentioned here are all finite dimensional and well defined [3].

2.3 Continuum Massless Scalar Fields on the 2D Causal Diamond

As we now have a consistent definition for the ground state of a massless scalar field in both the continuum and causal set framework, namely the SJ vacuum state, we will review the comparison between the continuum and causal set expressions for the SJ Wightman function on a 2D causal diamond, as done in [3]. Two sub-regions were explored, namely the center of the causal diamond and the corner, corresponding to Minkowski and Rindler space-times respectively. We start with the familiar metric on a two dimensional Minkowski space-time with coordinates (t,x) given by,

$$ds_M^2 = -dt^2 + dx^2 \tag{2.12}$$

and the massless scalar field equations,

$$\Box_M \phi = -\partial_t^2 \phi + \partial_x^2 \phi = 0 \tag{2.13}$$

We can separate the solutions to this equation in positive and negative frequencies and once again define the vacuum state $|0_M\rangle$ as the state annihilated by the operator version of the positive frequency modes in the Fourier expansion of $\hat{\phi}$. The Wightman function with respect to this vacuum state is given by,

$$W_M(t,x;t',x') = \langle 0_M | \, \hat{\phi}(t,x)\hat{\phi}(t',x') \, |0_M\rangle = \frac{1}{4\pi}\int_{-\infty}^{\infty} \frac{dk}{|k|} e^{-i|k|(t-t')+ik(x-x')} \tag{2.14}$$

which is logarithmically divergent at $k = 0$. As done in [3], the divergence can be removed by introducing an infrared momentum cutoff λ so that (2.14) can be evaluated as,

$$\begin{aligned} W_M(t,x;t',x') &= \frac{1}{4\pi}\int_{-\infty}^{\infty} \frac{dk}{|k|} e^{-i|k|(t-t')+ik(x-x')}\theta(|k|-\lambda) \\ &= -\frac{1}{2\pi}\ln(\mu|d|) - \frac{i}{4}\mathrm{sgn}(\Delta t)\theta(\Delta t^2 - \Delta x^2) + O(\lambda\Delta) \end{aligned} \tag{2.15}$$

where $\mu = \lambda e^{\gamma}$, γ is the Euler-Mascheroni constant, $\Delta t = t - t'$, $\Delta x = x - x'$ and $d = \sqrt{-\Delta t^2 + \Delta x^2}$. Dropping the $O(\lambda)$ term, $W_{M,\lambda}$ is defined as,

$$W_{M,\lambda} = -\frac{1}{2\pi}\ln(\mu|d|) - \frac{i}{4}\mathrm{sgn}(\Delta t)\theta(\Delta t^2 - \Delta x^2) \tag{2.16}$$

Equation 2.16 then serves as an approximation to the massless SJ two point function in the centre of a flat causal diamond [3]. Working in lightcone coordinates $u = (t + x)/\sqrt{2}$ and $v = (t - x)/\sqrt{2}$, we start with a causal diamond centred at the origin $u = v = 0$ corresponding to the region $u, v \in (-L, L)$ as shown in Figure 2.1 and has a space-time volume of $V = 4L^2$. The full theoretical calculation was done in [3] to find the exact SJ Wightman function on the flat causal diamond starting with the Pauli-Jordan function [4],

$$i\Delta(u, v; u', v') = -\frac{i}{2}[\theta(u - u') + \theta(v - v') - 1] \tag{2.17}$$

It was found that the SJ Wightman function, $W_{SJ,L}$, was the same as the exact continuum two-point function of the ground state of a massless scalar field in a box with reflecting boundaries at $x = \pm\sqrt{2}L$ up to a correction term.

2.3.1 The Center Region

We wish to determine what the SJ Wightman function looks like in the large L limit as one would expect the boundary effects to become negligible and approximate the true vacuum of Minkowski space. As such, near the center of the causal diamond points are chosen so that,

$$|u - u'| \ll L, \quad |v - v'| \ll L, \quad |u - v'| \ll L, \quad |v - u'| \ll L \tag{2.18}$$

Following this approximation, the continuum Wightman function near the

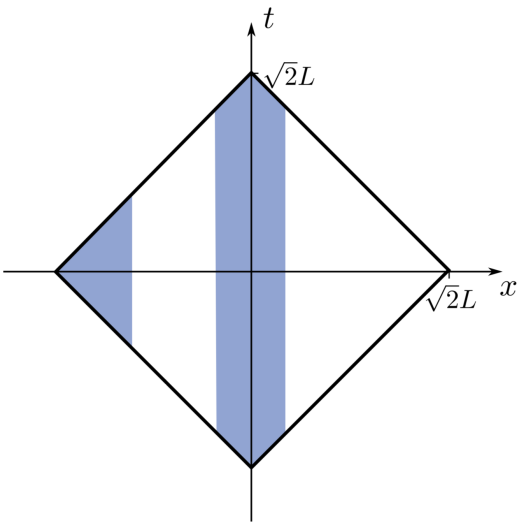

Figure 2.1: The 2D causal diamond [3]. The continuum analysis is carried out on the shaded center and corner regions.

center of the causal diamond is given by [3],

$$W_{\text{center}}(u,v;u',v') = -\frac{1}{4\pi}\ln(|\Delta u\Delta v|) - \frac{i}{4}\text{sgn}(\Delta u+\Delta v)\theta(\Delta u\Delta v) \\ -\frac{1}{2\pi}\ln\left(\frac{\pi}{4L}\right) + \epsilon_{\text{center}} + O(\frac{\delta}{L}) \tag{2.19}$$

where $\epsilon_{\text{center}} \approx -0.063$ is a correction term in the derivation and $|\Delta u\Delta v| = \frac{1}{2}|d|^2$. We then see that for large L this agrees with $W_{M,\lambda}$, the Minkowski Wightman function with cutoff λ in Equation 2.16. The specific value for the cutoff was given by [3],

$$\lambda = \frac{\pi}{4\sqrt{2}}\exp(-\gamma - 2\pi\epsilon_{\text{centre}})L^{-1} \approx 0.46 \times L^{-1} \tag{2.20}$$

This result demonstrates that by taking the large L limit of the causal diamond, the SJ state in the center then approximates that of a Minkowski vacuum as was expected.

2.3.2 The Corner Region

A similar analysis was also done on the corner region of the causal diamond corresponding to the Rindler space-time, starting with the Rindler metric [19][20],

$$ds_R^2 = e^{2a\xi}(-d\eta^2 + d\xi^2) \tag{2.21}$$

such that the coordinates (t, x) are related to (ξ, η) via the coordinate transformations,

$$t = a^{-1}e^{a\xi}\sinh a\eta \qquad x = a^{-1}e^{a\xi}\cosh a\eta$$

Here $a > 0$ is a constant with dimensions of inverse length, while ξ and η satisfy the conditions $-\infty < \xi, \eta < \infty$. ξ and η are coordinates covering the right Rindler wedge, $x > |t|$ shown in Figure 2.2. Lines of constant ξ represent the trajectories of observers moving with constant acceleration $ae^{-a\xi}$ [3]. Following a similar analysis as was done starting at Equation 2.14, the two point function is given by,

$$W_{R,\lambda}(\eta, \xi; \eta', \xi') = -\frac{1}{4\pi}\ln \mu^2|\Delta\eta^2 - \Delta\xi^2| - \frac{i}{4}\mathrm{sgn}(\Delta\eta)\theta(\Delta\eta^2 - \Delta\xi^2) \tag{2.22}$$

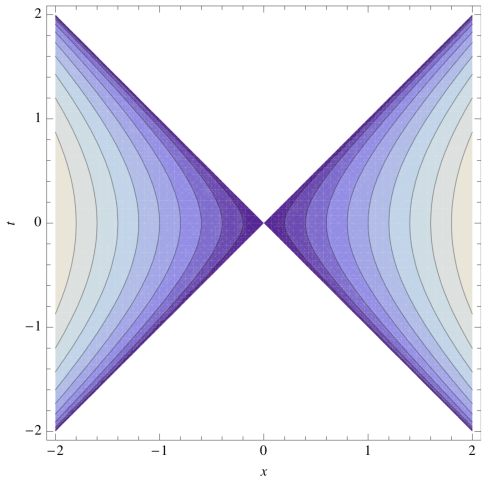

Figure 2.2: The left and right Rindler wedge [3]. The hyperbolic lines represent lines of constant ξ.

However, working once again with the SJ Wightman function $W_{SJ,L}$ and looking at this in the corner region for the $L \to \infty$ limit, it was shown to take the form,

$$W_{\text{corner}}(t, x; t', x') = W_{M,\lambda}(t, x; t', x') - W_{M,\lambda}(t, x; t', -x') \tag{2.23}$$

which does not resemble the form of $W_{R,\lambda}(\eta, \xi; \eta', \xi')$ in Equation 2.22. Instead this looks like the ground state of a scalar field with a mirror placed at the corner of the right Rindler wedge. Hence one finds that the vacuum state in the corner region of the causal diamond does not seem to resemble the Rindler vacuum as was expected. As was suggested in [3], a possible reason for this discrepancy is the fact that we are working with massless fields which would be able to 'sense' the boundaries of the region even in the $L \to \infty$

limit, although intuitively one would assume that the left corner would become unaware of the right mirror in the large L limit. This discrepancy will be of particular interest when we look to explore this region in the case of a three dimensional causal diamond.

2.4 The SJ Causal Set Wightman function

After establishing the continuum expressions for the SJ Wightman functions on the causal diamond for the two sub-regions in [3], these results were then compared to the causal set Wightman functions calculated directly from the points in the causal diamond using the formalism developed in chapter one. Starting with a sprinkling of points in the causal diamond C_L, the massless retarded propagator K_R can be calculated using the Equation 1.33 and setting $\Phi = \frac{1}{2}C$ [14],

$$K_R = \frac{1}{2}C \tag{2.24}$$

where C is the causal matrix. From this the Pauli-Jordan function $i\Delta$ can be calculated using

$$i\Delta = i(K_R - K_R^T) \tag{2.25}$$

As described earlier the positive part of $i\Delta$ is then equated to the causal set Wightman function $w^{ij} = w(v_i, v_j)$ for $v_i, v_j \in C_L$. We can compare this directly to the values of the continuum Wightman functions $W^{ij} = W(X_i, X_j)$ calculated in the previous section. The real parts of W and w were

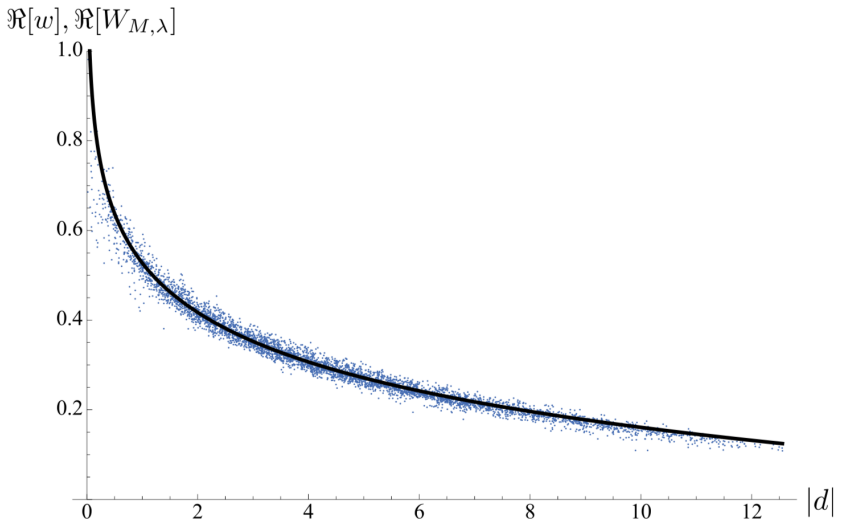

Figure 2.3: The real part of $W_{M,\lambda}(X, X')$ (black line) against the causal set SJ Wightman function w_{ij} in the center of causal diamond [3].

plotted against proper time $|d(X_i, X_j)|$ for time-like related points, where in the center, the real part of the continuum Wightman function with infrared cutoff $\lambda = 0.02$ was given by [3],

$$R[W_{M,\lambda}(x, y)] = -\frac{1}{2\pi} \ln(|d(x, y)|) + 0.53 \tag{2.26}$$

The plot for this against the causal set Wightman function is shown in Figure 2.3 above, taken from [3], where we can see there was a strong agreement between the values of the two functions. Similarly, the comparison between the causal set SJ Wightman function and the continuum Wightman function was also explored in the corner of the causal diamond. The causal set Wightman function was compared to various candidate continuum functions mentioned earlier, namely the SJ, Minkowski, left mirror and Rindler two point func-

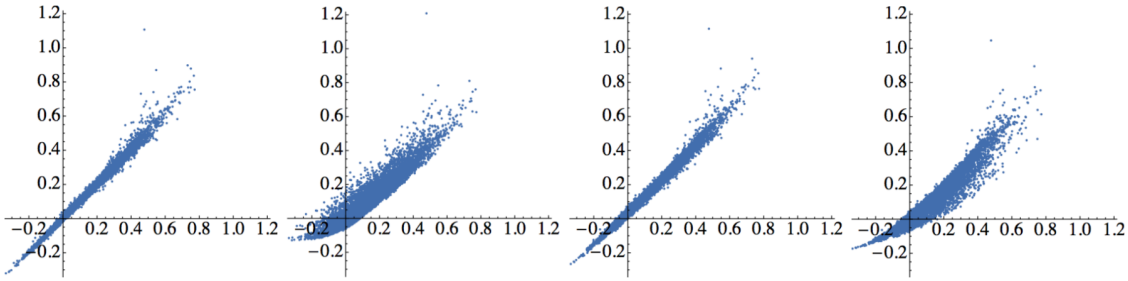

Figure 2.4: Correlation plots for the two-point functions in the corner of the causal diamond with w^{ij} on the horizontal axis and W^{ij} on the vertical [3].

tions. The comparison was done via correlation plots as the continuum two point functions were functions of more variables than just the proper time. In a correlation plot, the continuum value of the Wightman function $W^{i,j}$ is directly plotted against the discrete value $w^{i,j}$. The plots for these are taken from [3] and shown above in Figure 2.4, where going left to right we have the SJ, the Minkowski, the mirror, and the Rindler two-point functions. As we can see, there is a very close agreement between both the SJ and the mirror plots, confirming that vacuum in the corner region is indeed closer to the mirror function than what would intuitively be expected to be the Rindler Wightman function. Hence it was the shown the continuum calculation for the SJ state in the Rindler wedge doesn't agree with the limiting procedure used when constructing the finite diamond and letting the size of the diamond tend to infinity. A possible explanation for this was suggested in [3] relating to the infrared divergences of the two dimensional massless theory. In the next chapter we will explore whether this behavior is also observed in the case of three space-time dimensions.

Chapter 3

The SJ Vacuum in 3D

In this chapter, we aim to extend some of the numerical work done in [3] to the case of a three dimensional causal diamond. In three dimensions the diamond will look like a double cone joined by their circular base of radius r, centered at the origin. We once again want to determine the SJ ground state in the center of the causal diamond and in the wedge region, which as we saw in the previous chapter, we would have expected to correspond to the Minkowski and Rindler vacuums respectively, in the large diamond limit. The way we try to simulate this limit will involve trying to pick small enough subregions so that the boundary of the full diamond has a minimal effect.

3.1 The Setup

As we will be working in $d = 3$ space-time dimensions, to generate the 3-dimensional causal set C_D, we start off by sprinkling points into a cube of side length $l = 2$ centered at the origin. This is done by sampling each of the (x, y, t) coordinates from a uniform distribution on the interval $[-1, 1]$. We then keep points within the causal diamond centered at the origin, described by the region,

$$\left\{t < \frac{l}{2} - \sqrt{x^2 + y^2}\right\} \bigcap \left\{t > \sqrt{x^2 + y^2} - \frac{l}{2}\right\}$$

This is shown below in Figure 3.1. The number of points inside the causal diamond is thus approximately Poisson distributed around the mean $N_D = \rho_C V_D$, where N_D is the number of points inside the causal diamond, ρ_C is the sprinkling density into the cube and V_D is the volume of the causal diamond. The time coordinate on the vertical axis will once again provide a natural labelling for the points inside the causal diamond. We can then calculate the proper time τ_{ij} between pairs of points $v_i, v_j \in C_D$ and use the fact that if $\tau_{ij} > 0$ then the points are time-like separated, and hence causally related, while if $\tau_{ij} < 0$ we know the points are space-like separated and hence causally unrelated. We can then calculate C and L, the causal and link matrices respectively, from the causal diamond using the setup from chapter one.

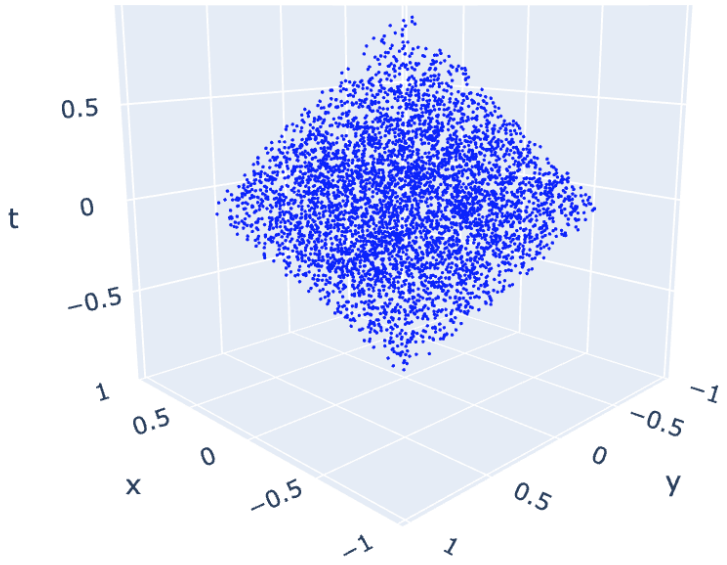

Figure 3.1: A sprinkling into a 3D causal diamond.

3.2 Propagators and Wightman functions

Once we have the Causal and Link matrices, we calculate the causal retarded Greens function K_R on the full causal diamond using Equation 1.11 in chapter one. As we are only working with massless fields, this expression simplifies giving $K_R = \Phi$, where in $d = 3$ space-time dimensions Φ is defined as [14],

$$\Phi_{xy} = \begin{cases} \frac{1}{2\pi}\left(\frac{\pi\rho_C}{12}\right)^{\frac{1}{3}}((C+I)^2)_{xy}^{-\frac{1}{3}} & \text{if } v_x \prec v_y \\ 0 & \text{otherwise} \end{cases} \tag{3.1}$$

Here the sprinkling density ρ_C is given by $\rho_C = N_C/V_C$. We can check the agreement between the causal set Greens function and the continuum Greens

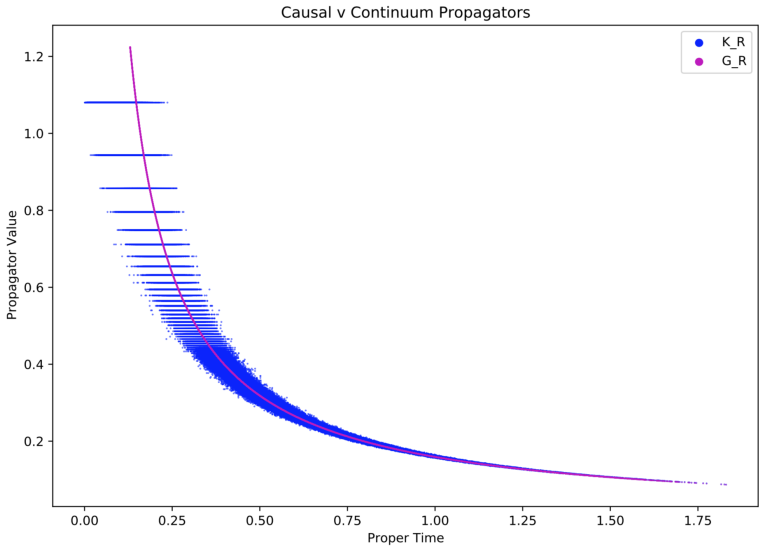

Figure 3.2: Plot of causal set versus continuum propagators.

function by comparing K_R to the expression for the continuum retarded Greens function in (1.19) given by,

$$(G_R)_0^{(3)}(x) = \theta(t)\theta(\tau^2)\frac{1}{2\pi\tau} \tag{3.2}$$

This is shown in Figure 3.2, where the blue points represent the causal set Greens function and the purple represent the continuum values. Equation 3.2 is derived in [14] by assuming the proper time is proportional to the cube root of the causal set volume between two points, however one can also calculate K_R using a different method, using the length of the longest chain. This uses the fact that the length of the longest chain between two causal set points v_x and v_y, denoted by l_{xy}, is proportional to the proper time between

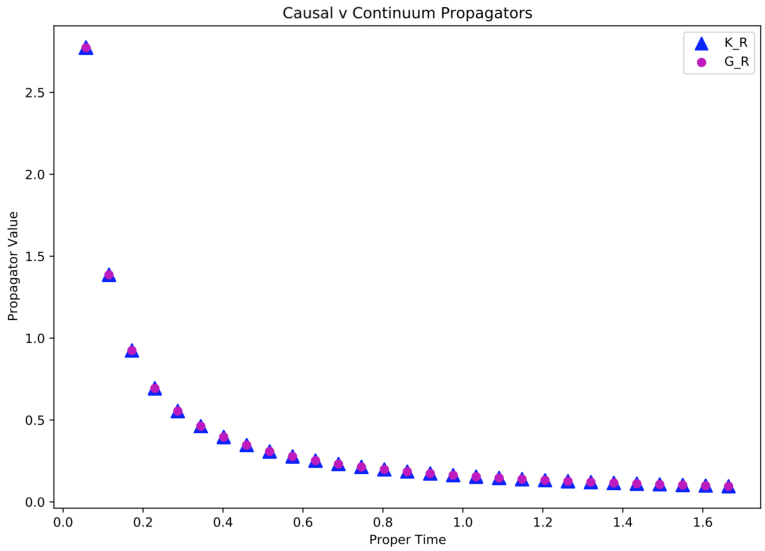

Figure 3.3: Plot of causal and continuum propagators via the length of the longest chain method.

them [18] [6]. The proper time τ is then related to l_{xy} through the equation,

$$\tau = \lim_{\rho \to \infty} \langle l_{xy} \rangle \left(\frac{\pi \rho}{12} \right)^{-\frac{1}{3}} \frac{1}{m_3} \tag{3.3}$$

where the brackets $< . >$ denotes the mean over the entries of l_{xy}, while m_3 is given by the equation [25],

$$m_3 = \lim_{\rho \to \infty} \langle l_{xy} \rangle \, (\rho V)^{-\frac{1}{3}} \tag{3.4}$$

so that it lies in the range $1.77 \leq m_3 \leq 2.62$ [18]. For our calculations, we will use the average value of m_3 in range mentioned above, namely $m_3 = 2.19$. This then gives an alternative definition for the retarded causal set

propagator [18],

$$(\widetilde{K_R})^{(3)}_{xy} = \begin{cases} \frac{1}{2\pi l_{xy}} \left(\frac{\pi\rho}{12}\right)^{\frac{1}{3}} & \text{for } v_x \prec v_y \\ 0 & \text{otherwise} \end{cases} \tag{3.5}$$

Once we have the propagator we can calculate the Pauli-Jordon function using definition (1.33), and hence obtain $i\Delta$. By using the spectral decomposition in (1.38), we obtain the Wightman function, w^{ij}, on the full causal diamond by taking the positive part as in Equation 1.39.

3.3 The SJ Vacuum in the Center

The first subregion we wish to explore is the center of the causal diamond. In order to approximate the vacuum of flat Minkowski space, we must look at a subdiamond in the center of the full causal diamond that, as mentioned earlier, is small enough that the role of boundary effects is negligible. If the full causal diamond has radius $r = 1$, we choose a sub-diamond of radius $r = 0.4$, so the volume of the subdiamond represents 6.4% of the full diamond. We then calculate the Wightman function w on the subdiamond by only keeping entries in the Wightman function matrix corresponding to points inside the subdiamond. We then compare this to the continuum Wightman

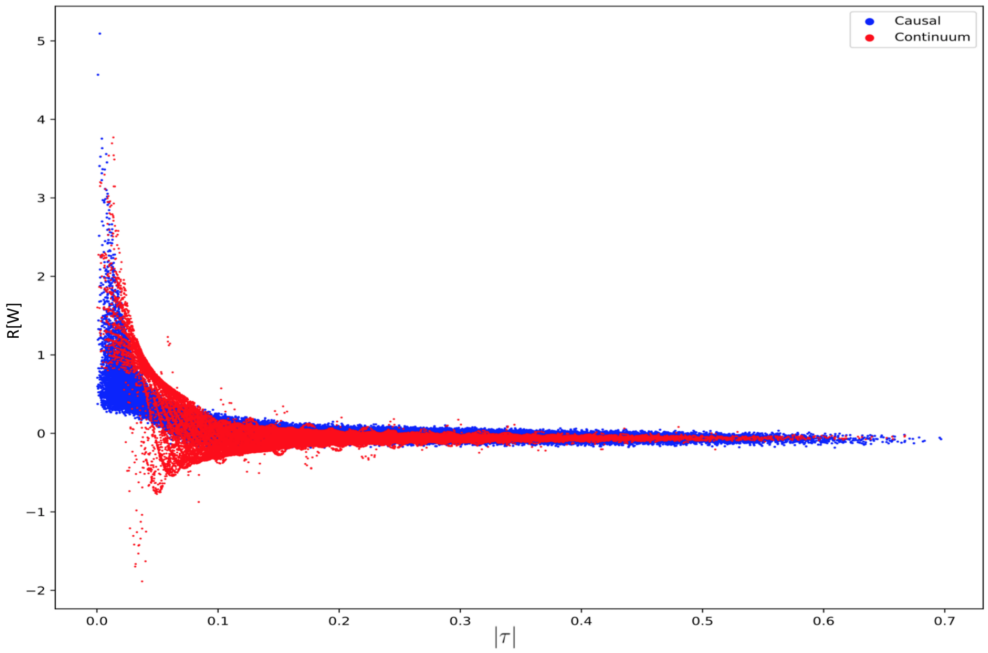

(a) Time-like points

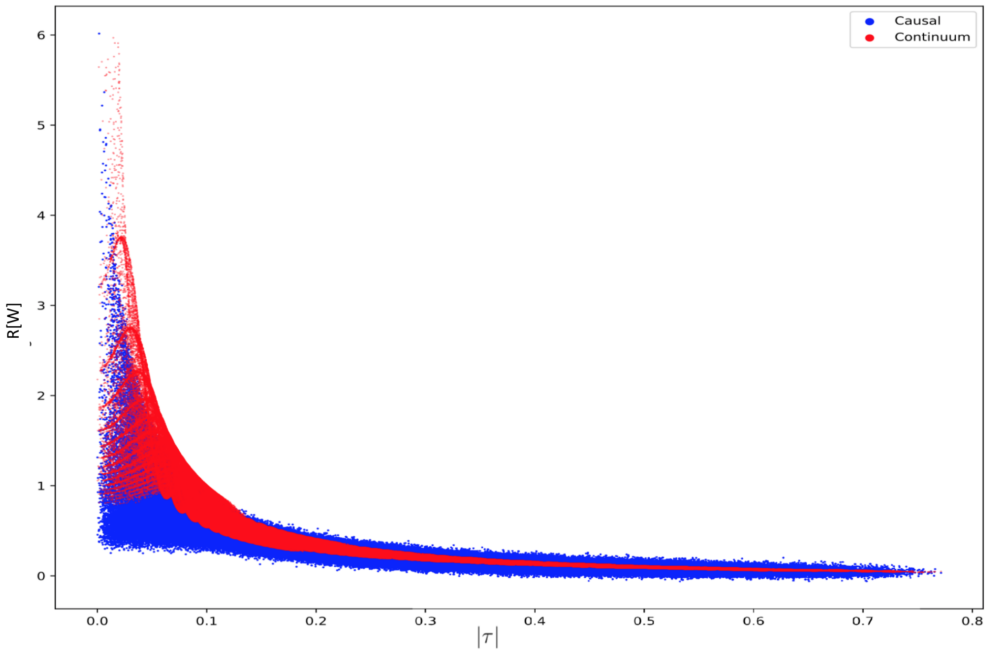

(b) Space-like points

Figure 3.4: Causal set versus continuum Wightman functions in the center region. Here τ is the proper time and $R[W]$ is the real part of the Wightman function.

function on a three dimensional Minkowski spacetime given by [21],

$$W_{\text{mink}}(x,x') = \frac{|\boldsymbol{x}-\boldsymbol{x'}|^{1-\frac{D}{2}}}{2(2\pi)^{\frac{D}{2}}}\int_0^\infty du \frac{u^{\frac{D}{2}}}{\sqrt{u^2+m^2}} J_{\frac{D}{2}-1}(u|\boldsymbol{x}-\boldsymbol{x'}|)e^{-i\sqrt{u^2+m^2}(t-t')} \tag{3.6}$$

where here $D = 2$ is the spatial dimension and $m = 0$ as we are working in the massless case. $J_\alpha(x)$ is the Bessel function of the first kind and the bold vectors here represents only the spatial components of the vector. As was done in the case of the two dimensional causal diamond, we introduce a ultraviolet and infrared cutoff, where the instead of having the integral limits as zero and infinity, for the numerical computation of Equation 3.6 we replace these with $\pi/4$ and 133 respectively. The comparison between $W_{\text{mink}}(v_i, v_j) = W^{ij}_{\text{mink}}$ and $w(v_i, v_j) = w^{ij}$ for $v_i, v_j \in C_D$ is shown in Figure 3.4 on the previous page, where a total of $N = 20,000$ points were used in the full causal diamond. The real part of the Wightman functions were plotted for two cases, depending on whether the causal set points were space-like separated or time-like separated. We see close agreement between the two functions for large proper times, however for very short proper times the two functions differ significantly. We also see this in the correlation plots in Figure 3.5 where the causal set SJ Wightman function is plotted on the horizontal axis and the Minkowski Wightman function on the vertical. We see there is an obvious positive correlation, however this is not as tight as what we saw in the two dimensional case. This might partially be due to the cutoffs used, as using different values for the cutoffs may provide a better

fit between the two functions. Despite the discrepancy at the small proper time scale, the SJ causal set Wightman function does seem to bear close resemblance to the Minkowski Wightman function in this region.

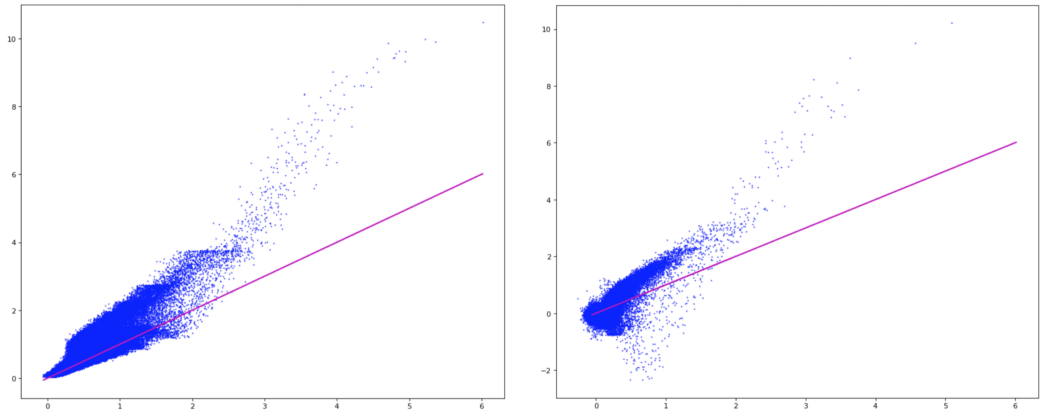

Figure 3.5: Correlation plots of the causal set versus Minkowski Wightman function. The left diagram is for the time-like separated points while the right for space-like separated points.

3.4 The SJ Vacuum in the Wedge

We now shift our analysis to the wedge region of the causal diamond. Recall that in the two dimensional case explored in [3], the SJ state was expected to resemble the Rindler vacuum, however, it seemed to more closely resemble the Minkowski space-time with a static mirror on the corner. In this section we explore whether this might be the case in the three space-time dimensions as well. We do a comparison between three different vacuua, characterised by the Rindler, Minkowski and Mirror Wightman functions W_{rind}, W_{mink} and W_{mirr} respectively. To define the wedge region, we shift our coordinate

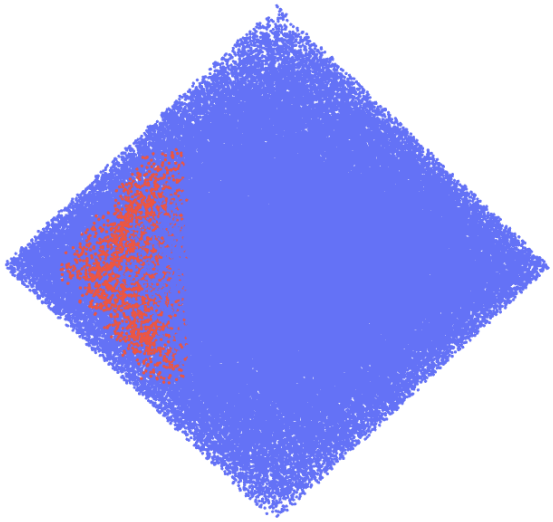

Figure 3.6: The three dimensional causal diamond with points in the wedge region highlighted in red.

axis so the "corner" lies at the origin. For our numerical calculations, we look at a thickened two dimensional slice extending 0.4 of the way along the radii towards the centre of the diamond. We use a thickened wedge, as a flat plane would have a zero probability of finding points on the plane in three dimensions. We set the thickness of the wedge to $\epsilon = 0.1$ and work with $25,000$ points in the causal diamond as this gives us approximately 380 points in the wedge region. The large number of causal set points required to obtain enough points in the wedge makes it challenging to obtain a definitive answer as to what the SJ vacuum state looks like, however we do review the preliminary results. The origin is placed at the right Rindler wedge, such that $x_1 > t$ and the Rindler coordinates $(\tau, \xi, \boldsymbol{x})$ are related to the Minkowski

coordinates $(t, x_1, \boldsymbol{x})$ by [22],

$$t = \xi \sinh \tau, \qquad x_1 = \xi \cosh \tau \tag{3.7}$$

W_{mink} is the same as Equation 3.6 above, while W_{rind} is given by [22],

$$W_{\text{rind}}(x, x') = W_{\text{mink}}(x, x') - \frac{1}{2\pi} \int_{-\infty}^{\infty} \frac{du}{\pi^2 + u^2} \left(\frac{m}{2\pi\gamma_1} \right)^{\frac{D-1}{2}} K_{(D-1)/2}(m\gamma_1) \tag{3.8}$$

where $K_\alpha(x)$ is the modified Bessel function of the second kind and γ_1 satisfies the condition,

$$\gamma_1^2 = \xi^2 + \xi'^2 + 2\xi\xi' \cosh(y - \tau + \tau') + |\boldsymbol{x} - \boldsymbol{x'}|^2 \tag{3.9}$$

In our three dimensional case, $x_1 = x$ and $\boldsymbol{x} = y$. Finally, W_{mirr} takes a similar form to Equation 2.23,

$$W_{\text{mirr}}(\boldsymbol{x}, t; \boldsymbol{x'}, t') = W_{\text{mink}}(\boldsymbol{x}, t; \boldsymbol{x'}, t') - W_{\text{mink}}(\boldsymbol{x}, t; -\boldsymbol{x'}, t') \tag{3.10}$$

We can see the comparison through the plots for these functions in Figure 3.7 and Figure 3.9 below, which compare the space-like and time-like separated points respectively. The correlation plots in Figure 3.8 are taken for proper times greater than 0.1 as this ignores large fluctuations coming from integrating over the Bessel functions at short proper times. Going from left to right in Figure 3.8 we have the correlation plots for the Minkowski,

Rindler and Mirror Wightman functions on the vertical axis, plotted against the SJ causal Wightman function on the horizontal axis for space-like separated points. Similarly, we also have the comparison for time-like separated points in Figure 3.9. Due to the heavily oscillatory behaviour of the time-like functions, correlation plots of these did not produce any meaningful way of making a comparison between the vacuum states. From these plots we can see that once again the Rindler and Mirror Wightman functions show the closest fit to the SJ causal set Wightman function. The plots seem to most closely support mirror behavior, as was observed in the two dimensional case, however, in order to definitively confirm this we must ultimately use larger causal sets.

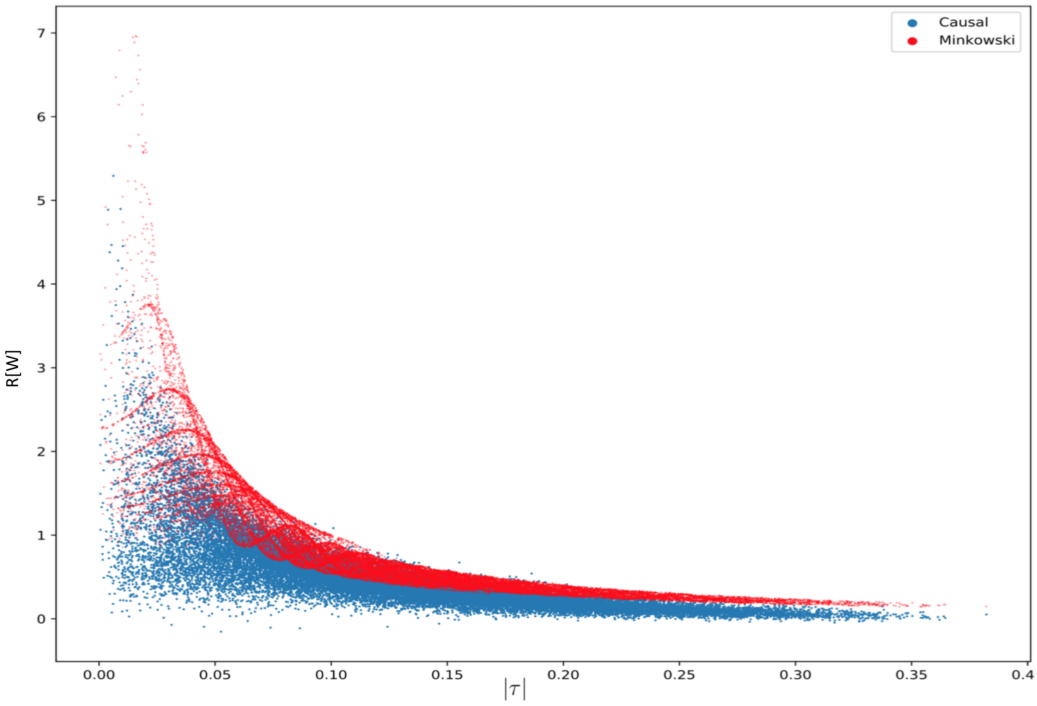

(a) Causal v Minkowski

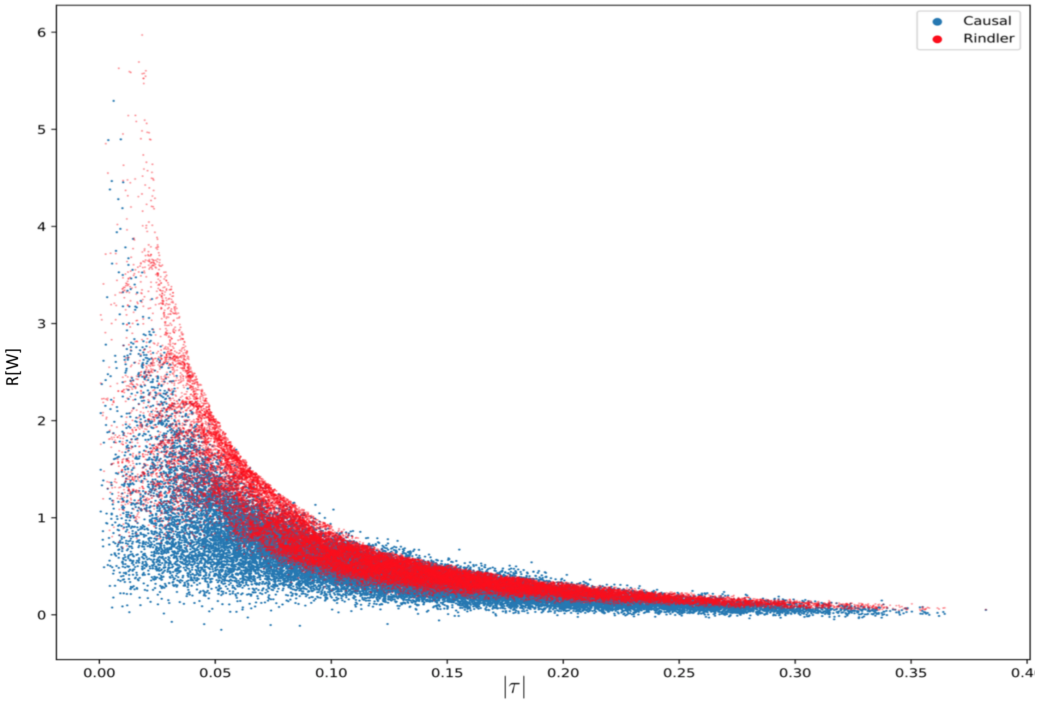

(b) Causal v Rindler

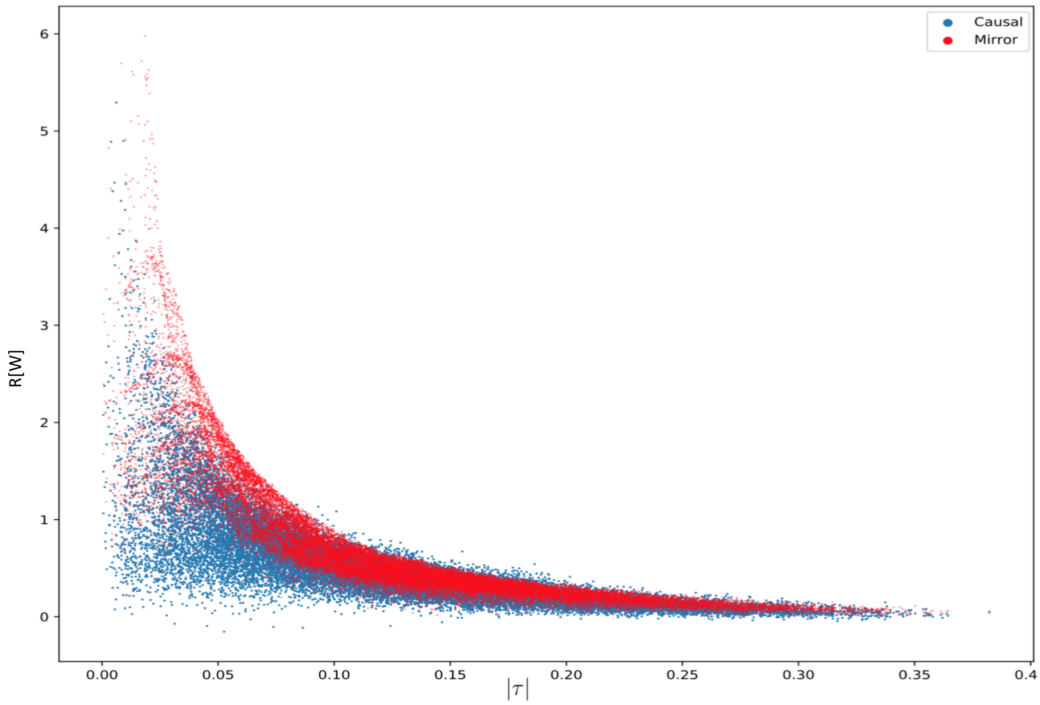

(c) Causal v Mirror

Figure 3.7: Plots of SJ causal set versus continuum Wightman functions for space-like separated points.

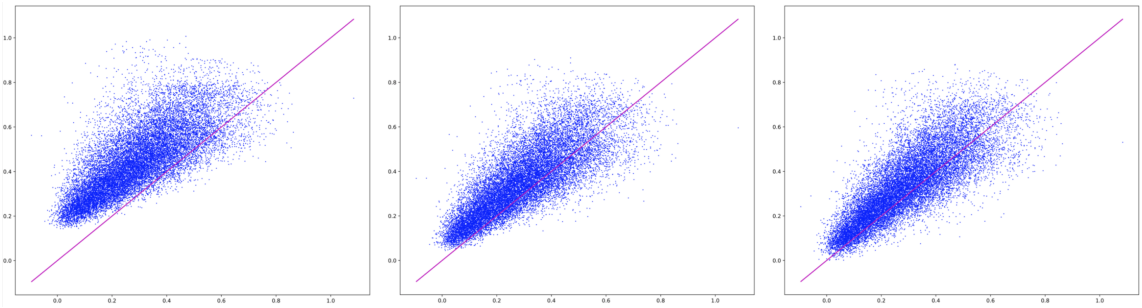

Figure 3.8: Correlation plots of, going left to right, W_{mink}, W_{rind} and W_{mirr}, for space-like separated points.

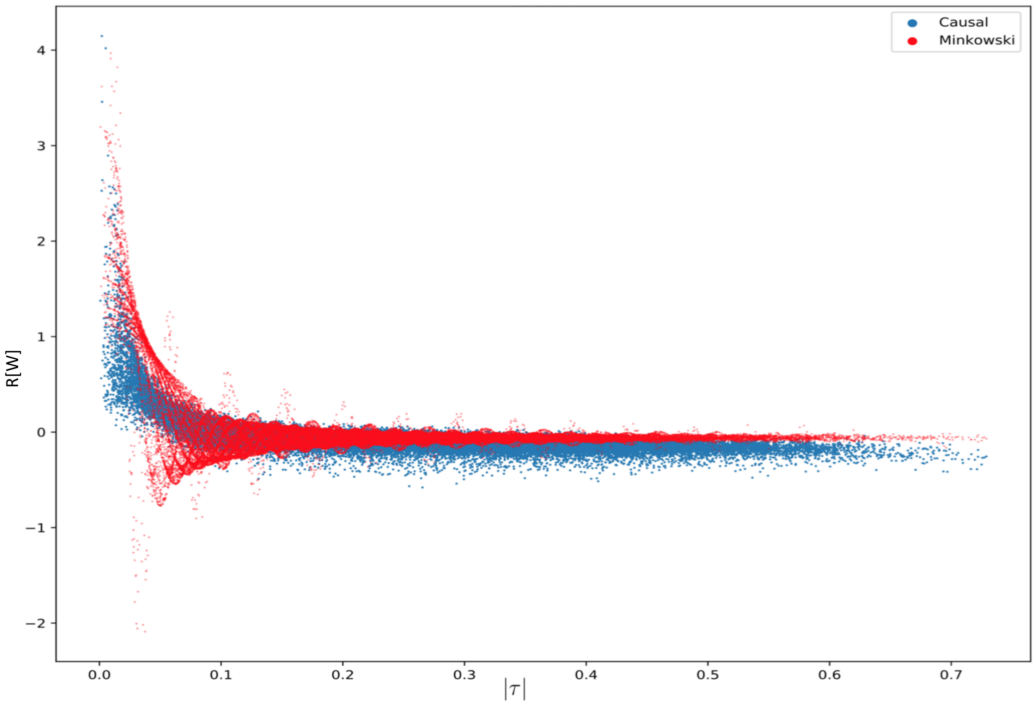

(a) Causal v Minkowski

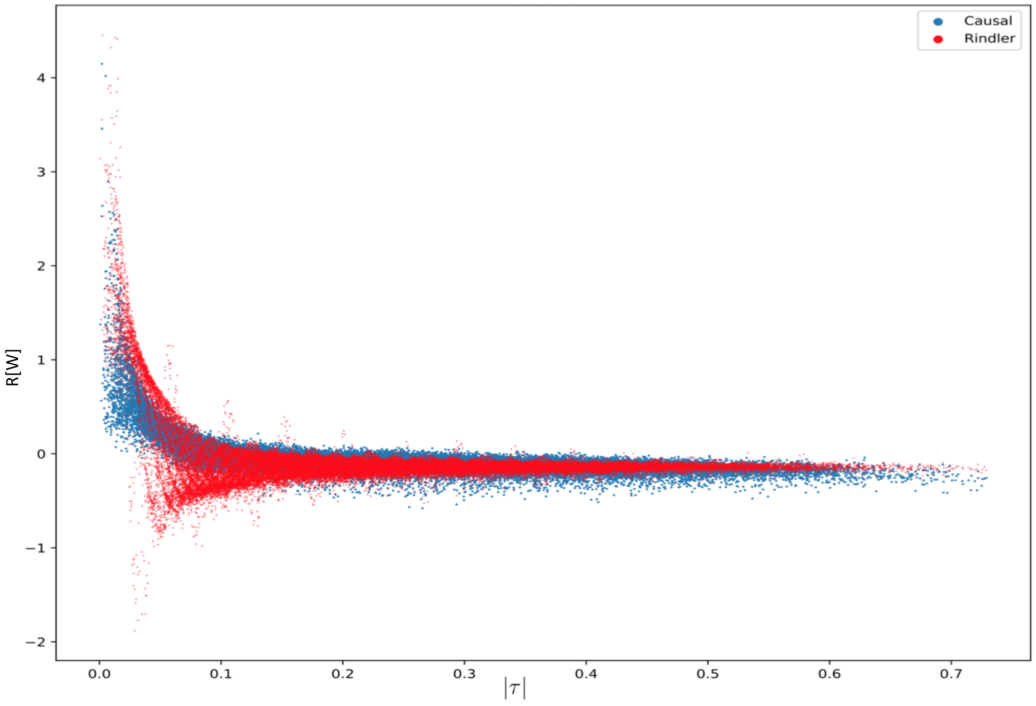

(b) Causal v Rindler

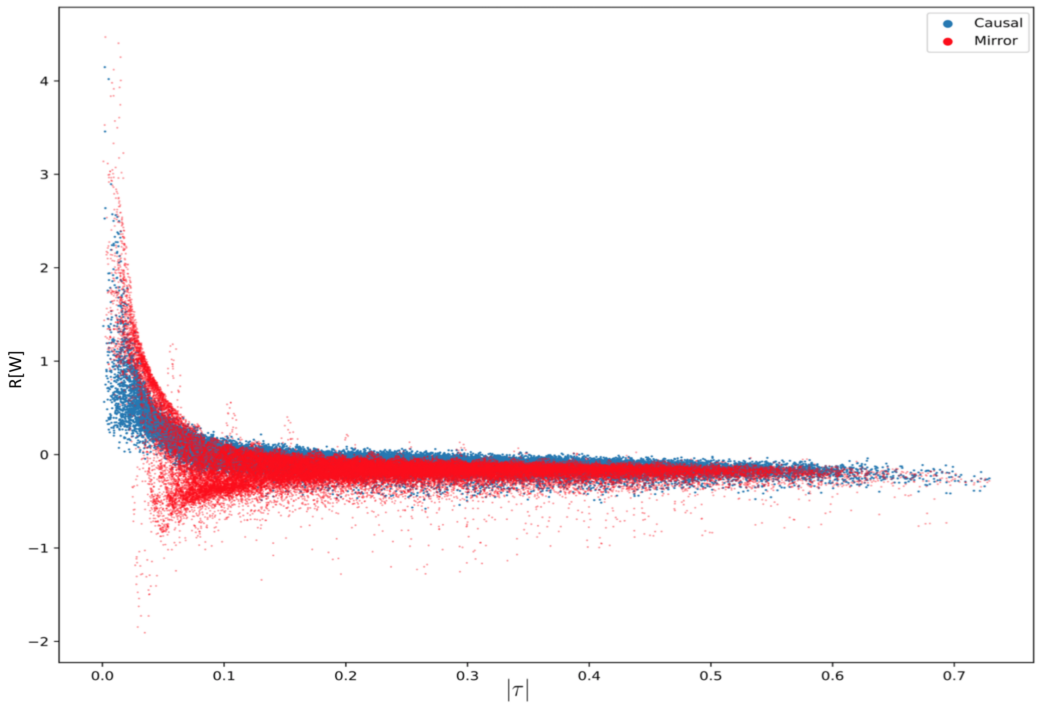

(c) Causal v Mirror

Figure 3.9: Plots of SJ causal set versus continuum Wightman functions for time-like separated points.

Chapter 4

Conclusion

To summarise the contents of this thesis, we started off by introducing the causal set approach to quantum gravity as a way of side stepping the conceptual difficulties and divergences found in traditional quantum field theory. The causal relations between discrete space-time points takes the center stage in this approach, and as we saw, this is almost enough to completely reconstruct Lorentzian space-time geometry. The discreteness scale acts as a natural barrier to the infrared and ultraviolet divergences found in traditional quantum field theory, however it also demands a new basis for quantisation. This was reviewed in chapter two, where we introduced the Sorkin-Johnston vacuum as an alternative distinguished vacuum state for a free scalar quantum field theory. Here the Pauli-Jordan function played a central role in the quantisation process and allowed us to avoid the ambiguity arising from defining positive frequency modes, whilst also making the quantisation pro-

cess intrinsically covariant. We looked at the consequences of this new ground state proposal by reviewing the work done in [3], where the SJ continuum Wightman functions characterising the SJ ground state was compared to the traditional vacuum state Wightman functions on the two dimensional causal diamond in the large L limit. The comparisons were also made to the causal set SJ Wightman function and it was found that while the SJ vacuum agreed with the expected Minkowski vacuum at the center of the causal diamond, it didn't match the expected result in the corner wedge region, which was expected to resemble the Rindler vacuum. Rather, it resembled the Minkowski vacuum with a mirror. In the final chapter we investigated this further in the case of a three dimensional causal diamond, where preliminary tests seem to show that the SJ vacuum in the wedge region once again resembles the Minkowski vacuum with a mirror rather than the Rindler vacuum. It was highlighted in [3] that ultimately the expressions used in the continuum comparison suffered from infrared divergences that were removed with a cutoff and perhaps a massive theory would result in a unique SJ state that agrees with the Rindler vacuum. These results provide a several possible routes for further research. First one could consolidate the preliminary results for the three dimensional diamond by working with larger causal sets, which may provide a more definitive answer regarding the SJ vacuum state in the wedge region. It may also be of interest to carry out a similar analysis in the case of a massive case to see whether this does indeed result in the SJ vacuum state resembling the Rindler vacuum.

Bibliography

[1] Gerard 't Hooft. "Quantum gravity: a fundamental problem and some radical ideas". In: *Recent Developments in Gravitation: Cargèse 1978* (1979), pp. 323–345.

[2] Niayesh Afshordi, Siavash Aslanbeigi, and Rafael D Sorkin. "A distinguished vacuum state for a quantum field in a curved spacetime: formalism, features, and cosmology". In: *Journal of High Energy Physics* 2012.8 (2012), pp. 1–29.

[3] Niayesh Afshordi et al. "A ground state for the causal diamond in 2 dimensions". In: *Journal of High Energy Physics* 2012.10 (2012), pp. 1–24.

[4] N. N. Bogoliubov, D. V. Shirkov, and Ernest M. Henley. "Introduction to the Theory of Quantized Fields". In: *Physics Today* 13.7 (1960), pp. 40–42. DOI: 10.1063/1.3057034. eprint: https://doi.org/10.1063/1.3057034. URL: https://doi.org/10.1063/1.3057034.

[5] Luca Bombelli et al. "Space-time as a causal set". In: *Physical review letters* 59.5 (1987), p. 521.

[6] Graham Brightwell and Ruth Gregory. "Structure of random discrete spacetime". In: *Physical review letters* 66.3 (1991), p. 260.

[7] WK Clifford. "On the hypotheses which lie at the bases of geometry". In: *General Theory of Relativity: The Commonwealth and International Library: Selected Readings in Physics* (2013), p. 107.

[8] David Finkelstein. "Space-time code". In: *Physical Review* 184.5 (1969), p. 1261.

[9] Stephen W Hawking, A Ro King, and PJ McCarthy. "A new topology for curved space–time which incorporates the causal, differential, and conformal structures". In: *Journal of mathematical physics* 17.2 (1976), pp. 174–181.

[10] Geoffrey Hemion. "A quantum theory of space and time". In: *Foundations of Physics* 10.11 (1980), pp. 819–840.

[11] Joe Henson. "The causal set approach to quantum gravity". In: *Approaches to quantum gravity: towards a new understanding of space, time and matter* 393 (2009).

[12] Steven Johnston. "Feynman propagator for a free scalar field on a causal set". In: *Physical review letters* 103.18 (2009), p. 180401.

[13] Steven Johnston. "Particle propagators on discrete spacetime". In: *Classical and Quantum gravity* 25.20 (2008), p. 202001.

[14] Steven Johnston. "Quantum fields on causal sets". In: *arXiv preprint arXiv:1010.5514* (2010).

[15] AV0637 Levichev. "Prescribing the conformal geometry of a lorentz manifold by means of its causal structure". In: *Soviet Math. Dokl.* Vol. 35. 452-455. 1987, p. 133.

[16] David B Malament. "The class of continuous timelike curves determines the topology of spacetime". In: *Journal of mathematical physics* 18.7 (1977), pp. 1399–1404.

[17] Jan Myrheim. "Statistical geometry, 1978". In: *CERN TH-2538* ().

[18] X Nomaan, Fay Dowker, and Sumati Surya. "Scalar field Green functions on causal sets". In: *Classical and Quantum Gravity* 34.12 (2017), p. 124002.

[19] Wolfgang Rindler. "Kruskal space and the uniformly accelerated frame". In: *American Journal of Physics* 34.12 (1966), pp. 1174–1178.

[20] Wolfgang Rindler. *Relativity: special, general, and cosmological*. 2003.

[21] AA Saharian. *" Quantum Field Theory In Curved Spacetime.*

[22] Aram A Saharian. "Polarization of the Fulling–Rindler vacuum by a uniformly accelerated mirror". In: *Classical and Quantum Gravity* 19.20 (2002), p. 5039.

[23] Rafael D Sorkin. "Scalar field theory on a causal set in histories form". In: *Journal of Physics: Conference Series*. Vol. 306. 1. IOP Publishing. 2011, p. 012017.

[24] Richard P Stanley. *Enumerative combinatorics. Vol. I, The Wadsworth & Brooks/Cole Mathematics Series, Wadsworth & Brooks*. 1986.

[25] Sumati Surya. "The causal set approach to quantum gravity". In: *Living Reviews in Relativity* 22.1 (2019), pp. 1–75.

[26] D Tong. "Quantum Field Theory: University of Cambridge Part III Mathematical Tripos. 2006". In: *URL http://www. damtp. cam. ac. uk/user/tong/qft. html* ().

[27] Erik Christopher Zeeman. "Causality implies the Lorentz group". In: *Journal of Mathematical Physics* 5.4 (1964), pp. 490–493.